Available online at www.sciencedirect.com
SCIENCE DIRECT®

TECTONOPHYSICS

Tectonophysics 420 (2006) 253–266

www.elsevier.com/locate/tecto

Crustal structure of the northeastern margin of the Tibetan plateau from the Songpan-Ganzi terrane to the Ordos basin

Mingjun Liu [a,b], Walter D. Mooney [b,*], Songlin Li [a,b], Nihal Okaya [b], Shane Detweiler [b]

[a] *Geophysical Exploration Center, China Earthquake Administration, 104 Wenhua Road, Zhengzhou, Henan 450002, China*
[b] *U. S. Geological Survey, 345 Middlefield Road, Menlo Park, CA 94025, USA*

Received 19 January 2005; received in revised form 17 October 2005; accepted 4 January 2006
Available online 5 May 2006

Abstract

The 1000-km-long Darlag–Lanzhou–Jingbian seismic refraction profile is located in the NE margin of the Tibetan plateau. This profile crosses the northern Songpan-Ganzi terrane, the Qinling-Qilian fold system, the Haiyuan arcuate tectonic region, and the stable Ordos basin. The P-wave and S-wave velocity structure and Poisson's ratios reveal many significant characteristics in the profile. The crustal thickness increases from northeast to southwest. The average crustal thickness observed increases from 42 km in the Ordos basin to 63 km in the Songpan-Ganzi terrane. The crust becomes obviously thicker south of the Haiyuan fault and beneath the West-Qinlin Shan. The crustal velocities have significant variations along the profile. The average P-wave velocities for the crystalline crust vary between 6.3 and 6.4 km/s. Beneath the Songpan-Ganzi terrane, West-Qinling Shan, and Haiyuan arcuate tectonic region P-wave velocities of 6.3 km/s are 0.15 km/s lower than the worldwide average of 6.45 km/s. North of the Kunlun fault, with exclusion of the Haiyuan arcuate tectonic region, the average P-wave velocity is 6.4 km/s and only 0.5 km/s lower than the worldwide average. A combination of the P-wave velocity and Poisson's ratio suggests that the crust is dominantly felsic in composition with an intermediate composition at the base. A mafic lower crust is absent in the NE margin of the Tibetan plateau from the Songpan-Ganzi terrane to the Ordos basin. There are low velocity zones in the West-Qinling Shan and the Haiyuan arcuate tectonic region. The low velocity zones have low S-wave velocities and high Poisson's ratios, so it is possible these zones are due to partial melting. The crust is divided into two layers, the upper and the lower crust, with crustal thickening mainly in the lower crust as the NE Tibetan plateau is approached. The results in the study show that the thickness of the lower crust increases from 22 to 38 km as the crustal thickness increases from 42 km in the Ordos basin to 63 km in the Songpan-Ganzi terrane south of the Kunlun fault. Both the Conrad discontinuity and Moho in the West-Qinling Shan and in the Haiyuan arcuate tectonic region are laminated interfaces, implying intense tectonic activity. The arcuate faults and large earthquakes in the Haiyuan arcuate tectonic region are the result of interaction between the Tibetan plateau and the Sino–Korean and Gobi Ala Shan platforms.

Keywords: China; Crustal structure; Deep seismic sounding; NE Tibetan plateau

1. Introduction

The NE margin of the Tibetan plateau, located in an important tectonic junction, is an ideal site to study continental dynamics. Much attention has been paid to the Tibetan plateau regarding its evolution as a product

* Corresponding author. Tel.: +1 650 329 4764; fax: +1 650 329 5163.
E-mail addresses: mliu@usgs.gov (M. Liu), mooney@usgs.gov (W.D. Mooney).

0040-1951/$ - see front matter © 2006 Published by Elsevier B.V.
doi:10.1016/j.tecto.2006.01.025

of the India–Asia collision (Molnar and Tapponnier, 1975). Since India collided with Asia ~55 million years ago, the Tibetan plateau has dominantly been growing toward the east and northeast (Tapponnier et al., 2001). Therefore, crustal structure and evolution in the NE plateau are attracting more attention (Cui et al., 1995; Herquel et al., 1995; Zhu and Helmberger, 1998; Meyer et al., 1998; Galve et al., 2002; Vergne et al., 2002; Pares et al., 2003).

A 1000-km-long geophysical profile was conducted from Darlag–Lanzhou–Jingbian extending from the Songpan-Ganzi terrane to the Ordos basin in the NE margin of the Tibetan plateau to study the interaction between the Tibetan plateau and the Sino–Korean platform, and to study the deep driving mechanisms of tectonic deformation (Fig. 1). It is a combination profile that consists of seismic refraction, teleseismic observation, and magnetotelluric soundings (MTS). In this

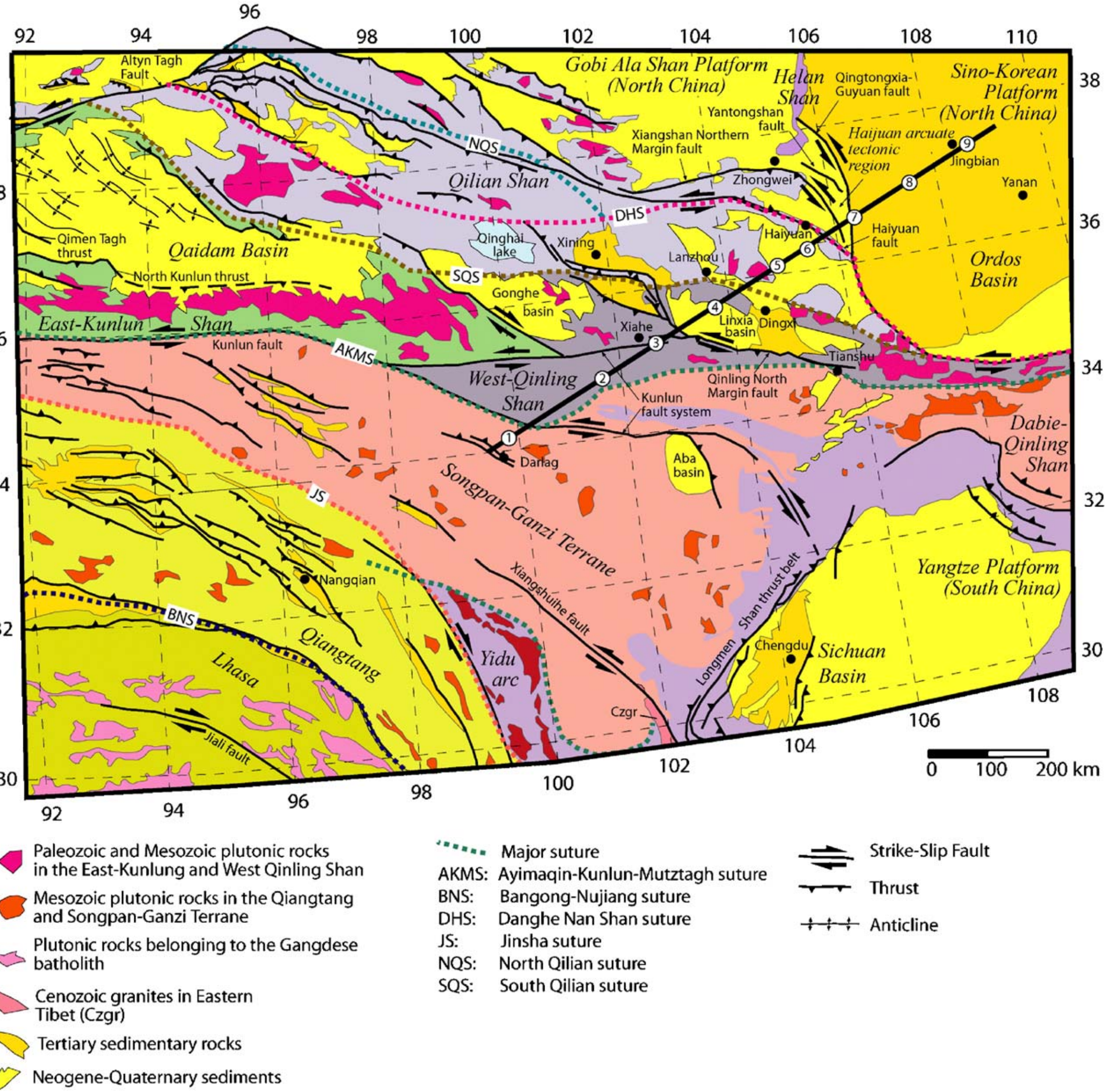

Fig. 1. Tectonic map of the NE Tibetan plateau (after Yin and Harrison, 2000). The seismic profile is indicated by a solid black line with circled numbers 1 through 9, indicating shot point locations. The southernmost shot point (SP1) is located in the Songpan-Ganzi terrane near Darlag. The northernmost shot point (SP9) is located in the Ordos basin near Jingbian. The seismic profile crosses the Qinling-Qilian fold system (SP2 to SP6) and the Haiyuan arcuate tectonic belt (SP7).

paper, we present the 2-D velocity structure from P- and S-waves, we infer the composition of the crust using Poisson's ratio, and we discuss the continental dynamics in the NE margin of the Tibetan plateau based on the seismic refraction data (Li et al., 2002; Liu et al., 2003).

2. Geologic setting

The study area covers the NE margin of the Tibetan plateau, and has a complicated geological background. It involves mainly three geological units, the northeastern Tibetan plateau, which includes the Songpan-Ganzi terrane, the Qinling-Qilian fold system, the Haiyuan arcuate tectonic region, the Ordos basin, in addition to two tectonic belts. The NS belt divides the Chinese continent into eastern and western tectonic provinces from the Helan Shan to the Sichuan-Yunnan (Li and Mooney, 1998), and the Central Orogenic Belt that divides the Chinese continent into northern and southern tectonic provinces along Kunlun–Qinling–Dabie (Jiang et al., 2000). Tectonic activity is very intense in the study area, where several $M \geq 8$ earthquakes have occurred in the past hundred years. Compression from the Indian plate has not only caused the crustal thickening and uplift of the NE Tibetan plateau, but has also affected adjacent areas such as the Sino-Korean platform and the Gobi Ala Shan platform. At the same time, the relatively solid blocks surrounding the plateau constrain the movement of the Tibetan plateau to some degree.

2.1. Songpan-Ganzi terrane (shot point SP1 in Fig. 1)

The Songpan-Ganzi terrane, which occupies a large part of the central Tibetan plateau, is a triangular tectonic element between the Qinling-Qilian fold system in the north and the Qiangtang terrane in the south. It is characterized by a thick sequence of Triassic strata of deep marine deposits. These Triassic strata are commonly referred to as the Songpan-Ganzi flysch complex, which was intensely deformed by folding and thrusting during the Late Triassic and Early Jurassic (Yin and Harrison, 2000). The southwestern end of the seismic profile extends into the Songpan-Ganzi terrane by about 50 km.

2.2. Qinling-Qilian fold system (West-Qinling Shan and Qilian Shan) (between shot point SP2 and SP6 in Fig. 1)

The Qinling-Qilian fold system is situated in the NE corner of the Tibetan plateau and is a fold-and-thrust system. Nowhere else does active overthrusting spread over a greater surface area ($\sim$500,000 km^2) than in the NE corner of Tibet (Tapponnier et al., 2001). This broad region of coeval mountain building is delimited by the Kunlun fault to the south, the Altyn Tagh fault to the northwest, and the Haiyuan fault to the northeast (Fig. 1). The most vigorously rising thrust-ranges along the eastern rim of Tibet lay north of the Kunlun fault (Tapponnier et al., 2001). The Kunlun fault separates the Songpan-Ganzi terrane from the Qinling-Qilian fold system which is divided into the West-Qinling Shan and the Qilian Shan by the Qinling north margin fault. The West-Qinling Shan is part of the Central Orogenic Belt in China.

2.3. Haiyuan arcuate tectonic region (shot point SP7 in Fig. 1)

The Haiyuan arcuate tectonic region connects three tectonic units: the Tibetan plateau in the southwest, the Sino–Korean platform in the northeast, and the Gobi Ala Shan platform in the north. It is also a junction of three intraplate blocks, similar to a triple junction that connects three plates (Tian and Ding, 1998). There are four arcuate faults in the region: the Haiyuan fault, the Xiangshan Northern Margin fault, the Yantongshan fault, and the Qingtongxia-Guyuan fault. The faults converge toward the southeast and diverge toward the northwest. Many large earthquakes occurred on the arcuate faults in the region, including the 1920 $M=8.5$ Haiyuan earthquake on the Haiyuan fault. The Haiyuan fault is the boundary of the northeastern Tibetan plateau. The NS belt passes through the Haiyuan arcuate tectonic region.

2.4. Ordos basin (Sino-Korean Platform) (between shot point SP8 and SP9 in Fig. 1)

The Ordos Basin is a Mesozoic basin in the Sino-Korean platform. The Sino-Korean platform is considered to be one of the most stable tectonic provinces in China (Yin, 2002). Its basement consists of Archean metamorphic rocks. The upper Proterozoic and the lower Palaeozoic layers are marine sediments, the Carboniferous layers are interbedded coal strata of marine and land sediments, and above the Permian layers are land sediments. The surface cover of the Ordos basin consists of thick Mesozoic and Cenozoic layers. There are few earthquakes in the central Ordos basin, in contrast to its margin, which further demonstrates the stability of this block.

3. Seismic data

3.1. Acquisition and processing

Along the Darlag–Lanzhou–Jingbian seismic profile, twelve charges were fired at nine shot points numbered SP1 to SP9 (Fig. 1). All charges were fired in boreholes except for the water shot at SP1. Each charge size was about 2 tons. The seismic energy was recorded by 200 portable digital seismographs, DAS-1, developed by the Geophysical Exploration Center of the China Earthquake Administration (CEA). Three-component geophones were used for the whole profile and the receiver spacing was 1.5–2 km. High quality P- and S-wave data were acquired.

The vertical-component and the horizontal-component parallel with the profile were used to identify P- and S-waves, respectively. Record sections were plotted with reduction velocities of 6.00 and 3.46 km/s for P- and S-waves, respectively. In order to match the P-wave arrival times, the timescale used for S-waves was compressed by a factor of 0.58 on the S-wave record section. To improve the signal-to-noise ratio, the data were filtered with band passes of 0–10 and 0–6 Hz, respectively, for P- and S-waves.

3.2. Correlation of phases

According to the kinetic and dynamic characteristics of seismic waves, and taking into consideration P- and S-wave data, eight P-wave (S-wave) phases, P_g (S_g), P_1P (S_1S), P_cP (S_cS), P_3P (S_3S), P_4P (S_4S), P_5P (S_5S), P_mP (S_mS) and P_n (S_n), were identified from

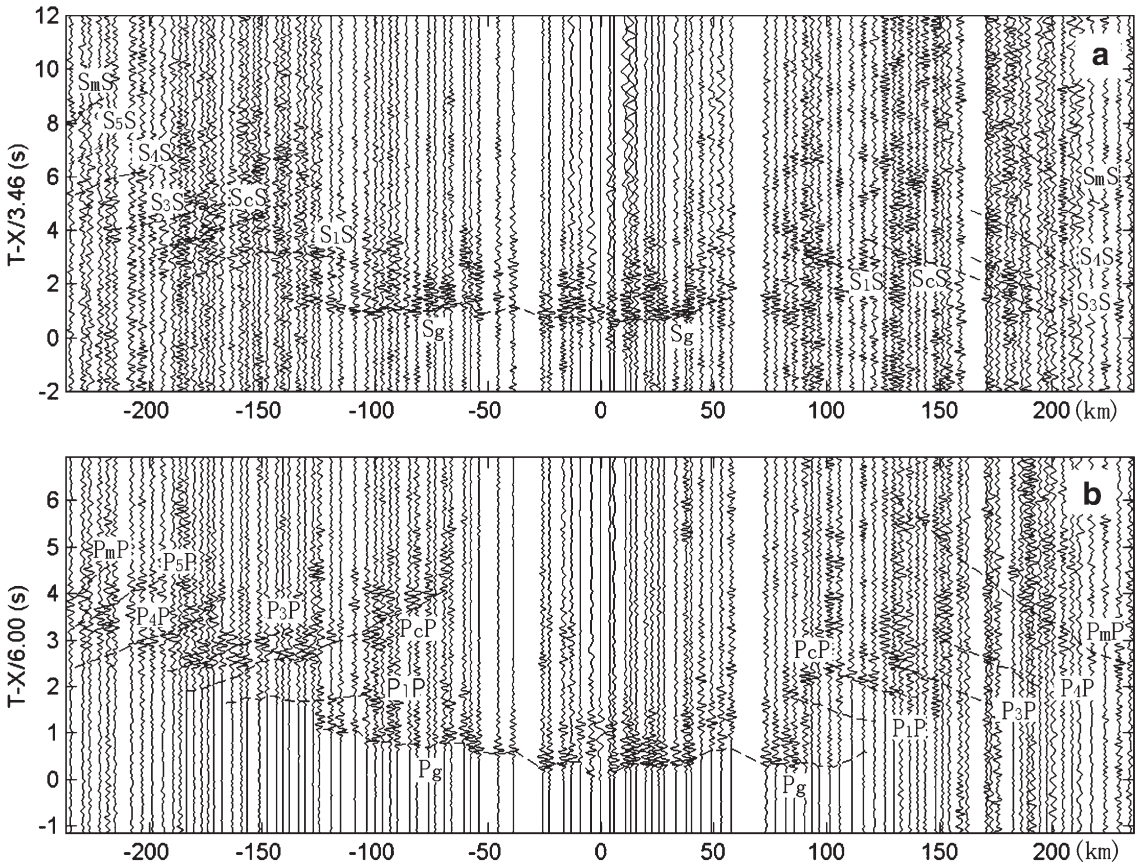

Fig. 2. Record sections of shot point SP2 located in the West-Qinling Shan of the Qinling-Qilan fold system. (a) Trace-normalized band-pass filtered (0–6 Hz) S-wave record section with a reduction velocity of 3.46 km/s and a factor of 0.58 in timescale with respect to P-wave record section; (b) Trace-normalized band-pass filtered (0–10 Hz) P-wave record section with a reduction velocity of 6.00 km/s. There are several reflections but the wide-angle reflections from the Moho (P_mP and S_mS) are not very clean. Arrival times of S-wave reflections are obviously later than that expected for a Poisson's ratio of 0.25. Seismic phases are labeled as: basement refraction (P_g and S_g) and reflections (P_1 and S_1, P_cP and S_cS, P_3 and S_3, P_4 and S_4, P_5 and S_5) from different depths.

record sections along the profile (Li et al., 2002; Liu et al., 2003). Not all phases could be identified in each tectonic unit.

The nomenclature of the phases identified in the data is as follows (Figs. 2–4). P_g (S_g) is a diving wave of the superficial sedimentary layer or basement cover, or the refraction from the basement. P_cP (S_cS) and P_mP (S_mS) are the reflections from the Conrad discontinuity and the Moho, respectively. P_n (S_n) refracts through the upper mantle. P_1P (S_1S), P_3P (S_3S), P_4P (S_4S) and P_5P (S_5S) are defined as intracrustal reflections.

Different phases have different strengths and characteristics along the profile. S-wave phases are not always as clear as P-wave phase due to a lower signal-to-noise ratio. P_g (S_g) is a clear phase that contains detailed information about near-surface sediments of the upper crustal velocity structure, and can be observed at a distance less than 150 km from the shot. P_mP (S_mS) is a relatively strong and continuous phase in the record sections. As a reflection from the Moho, P_mP (S_mS) usually appears at 80–120 km from the shot and can be observed as far away as 200 km from the shot (Figs. 3 and 4). The P_mP (S_mS) phase, observed from the record section of the northeasternmost shot point SP9 (Fig. 5) located in the Ordos basin, is very clear and has a simple waveform, large amplitude, sharp wavefront, and short duration. Conversely, the P_mP (S_mS) phase, detected in the western branch of the record section from SP7, lasts longer and has a complicated waveform. In general, it is relatively weak both in amplitude and energy observed in the southwestern record section of the profile (Fig. 2). In the record section of SP4 (Fig. 3b), the travel times of P_mP are obviously delayed at a distance greater than 170 km. This indicates that there is a deep crustal Low-Velocity-Zone (LVZ) in the West-Qinling Shan. In fact, different depths of the LVZ are observed in the segment. P_cP (S_cS) is the clearest phase after P_mP (S_mS) and P_g (S_g), and we infer that there is a Conrad discontinuity

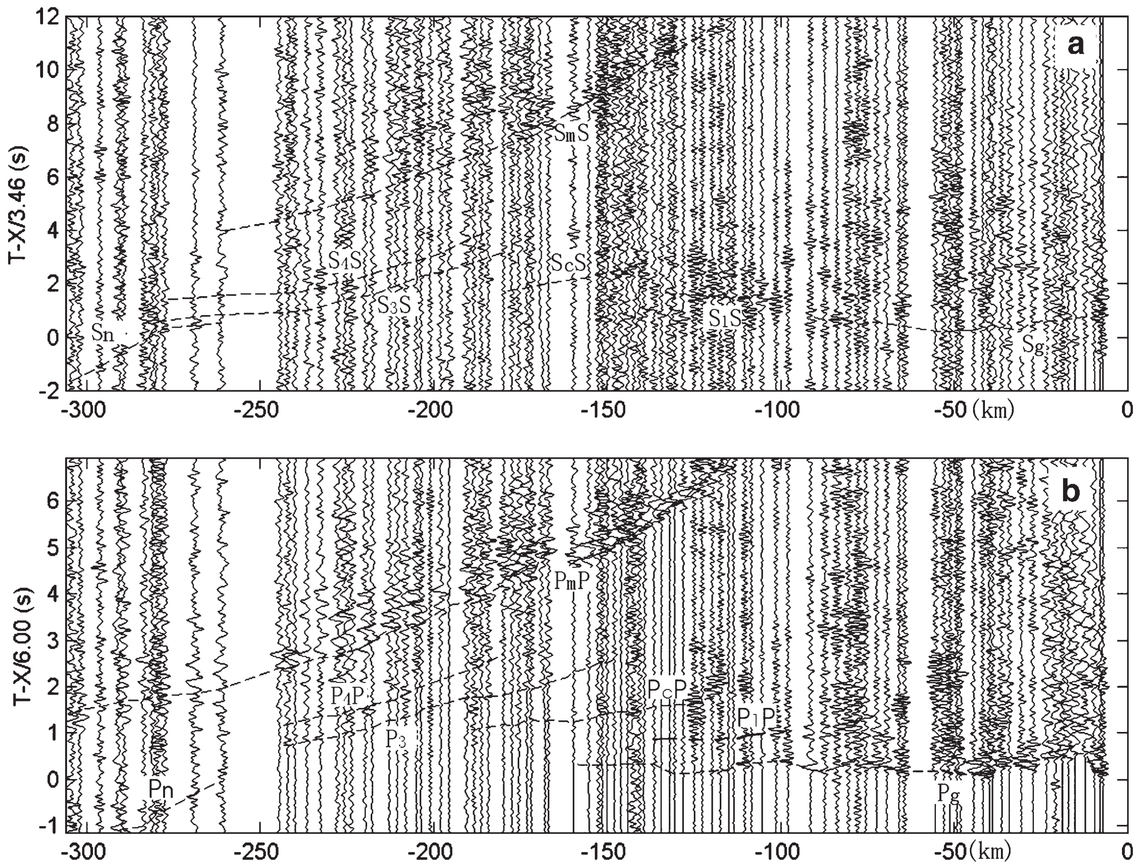

Fig. 3. Record sections of shot point SP4 located in the Qilian Shan of the Qinling-Qilan fold system. (a) Trace-normalized band-pass filtered (0–6 Hz) S-wave record section with a reduction velocity of 3.46 km/s and a factor of 0.58 in timescale with respect to P-wave record section; (b) Trace-normalized band-pass filtered (0–10 Hz) P-wave record section with a reduction velocity of 6.00 km/s. P_nP and S_nS are refractions from below the Moho and other seismic phases are labeled as in Fig. 2. The reflections from Moho (P_mP and S_mS) are very clear and the travel times of P_mP are obviously delayed at a distance greater than 170 km.

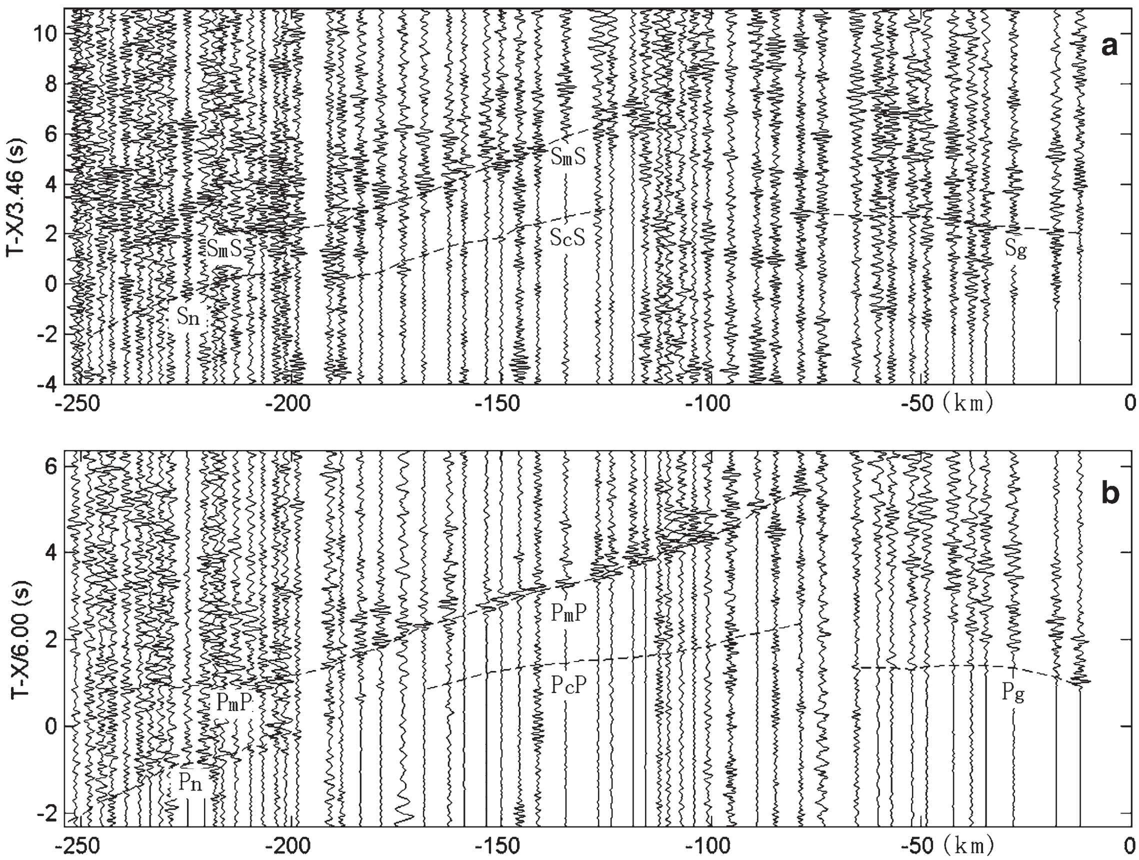

Fig. 4. Record sections of shot point SP9 located in the Ordos basin. (a) Trace-normalized band-pass filtered (0–6 Hz) S-wave record section with a reduction velocity of 3.46 m/s and a factor of 0.58 in timescale with respect to P-wave record section; (b) Trace-normalized band-pass filtered (0–10 Hz) P-wave record section with a reduction velocity of 6.00 km/s. Seismic phases are labeled as in Figs. 2 and 3. The reflections from Moho (P_mP and S_mP) and refractions from below Moho (P_nP and S_nS) are very clear.

dividing the crust. Some secondary reflections, P_1P (S_1S), P_3P (S_3S), P_4P (S_4S) and P_5P (S_5S), were observed, but were discontinuous and weaker than P_cP (S_cS). So we believe the upper crust and the lower crust were subdivided into different secondary layers in different tectonic units. An upper crustal LVZ was observed in the western branch of the record section of SP7, which corresponds to the Haiyuan arcuate tectonic region. P_nP (S_nP) was observed as the first arrival in several record sections at distances greater than 200 km (Figs. 4 and 5).

4. Modeling the data

Based on the above-mentioned phase correlations and in light of results from P-wave data processing and S-wave data processing, the two-dimensional P- and S-wave velocity structure and Poisson's ratio were established (Li et al., 2002; Liu et al., 2003).

The P-wave velocity structure was obtained by using P_cP and P_mP phases to determine the depths and average velocities of the Conrad discontinuity and Moho corresponding to each shot, applying the x^2-t^2method (Giese et al., 1976). Next, the P-wave velocity–depth function of each shot was obtained by one-dimensional reversion. The final two-dimensional P-wave velocity structure (Fig. 6a) was acquired after travel times and amplitudes of the various P-wave phases on the record sections were fitted by adjusting the velocities and depths of the boundaries (e.g., Fig. 5) in the initial model with two-dimensional forward raytracing (Cerveny et al., 1977; Cerveny and Psenick, 1984).

The S-wave velocity structure was determined on the basis of the P-wave model. At first, the depths to all boundaries were set at those distances obtained from the P-waves. Next, a two-dimensional initial inhomogeneous S-wave velocity model was constructed. Finally, the final two-dimensional S-wave model was acquired after travel times and amplitudes of the S-wave phases on the record sections were fitted by adjusting the velocities in the initial model using the raytracing method.

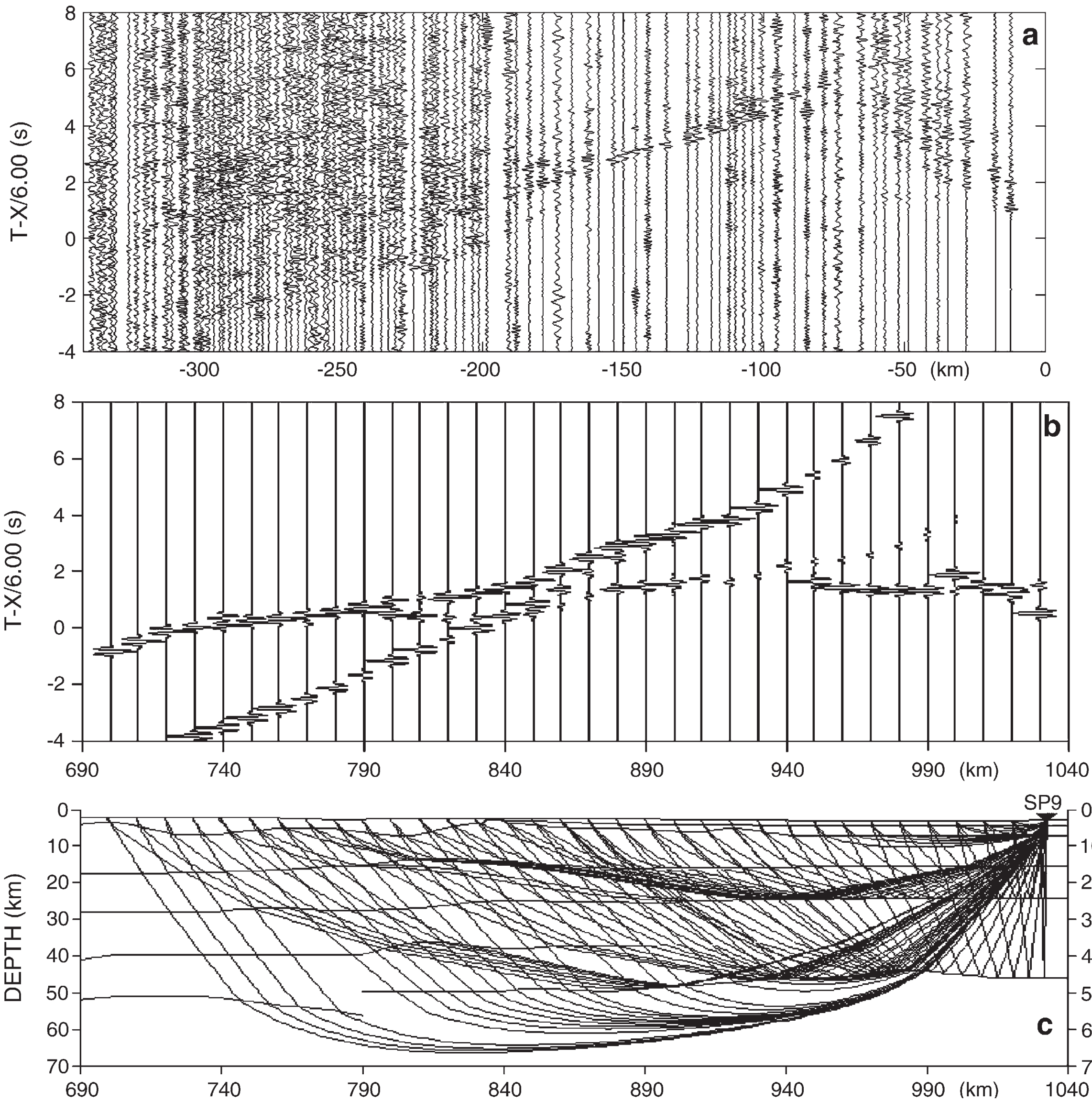

Fig. 5. (a) Observed and (b) synthetic record sections of P-waves and (c) ray coverage for SP9 located in the Ordos basin. The wide-angle reflection from the Moho (P_mP) and refractions from below Moho (P_n) are very clear.

Uncertainties in the final velocity model primarily depend on the correct identification of the various phases and the density of rays, the shot point interval, the receiver density, and the degree of lateral variations in the thickness of surficial sediments. Our result has shown that, depending on the uniformity of the structure and the density of the rays, the ability to resolve velocity and depths to the interfaces are 2% and 5%, respectively. Thus a velocity of 7.0 km/s has an uncertainty of ±0.14 km/s and a layer depth of 30 km has an uncertainty of ±1.5 km. The V_p/V_s ratio has an uncertainty of 4%. The final velocity structure including P-wave velocity, S-wave velocity and Poisson's ratio (Fig. 6) are discussed in the following sections.

4.1. P- and S-wave velocity structure

The crustal P- and S-wave velocity structure (Fig. 6a and b) shows crustal thickness variations along the profile. The crustal thickness increases gradually from 42 km beneath the Ordos basin in the northeast to 63 km beneath the Songpan-Ganzi terrane in the southwest. The average crustal thickness is 47 km beneath the Haiyuan arcuate tectonic region, 56 km beneath the

Qilian Shan, and 60 km beneath the West-Qinling Shan. The Conrad discontinuity (interface C in Fig. 6) marks the boundary between the upper and lower crust. Like the whole-crustal thickness, the upper- and lower-crustal thicknesses show as well a general increase in thickness from 17 km (respectively 21 km) beneath the Ordos basin to 25 km (respectively 38 km) beneath the Songpan-Ganzi terrane.

Crustal velocities vary considerably along the profile. The average crustal P-wave velocity (S-wave velocity) is 6.4 (3.7) km/s beneath the Ordos basin, 6.3 (3.5) km/s in the Haiyuan arcuate tectonic region, 6.4 (3.7) km/s in the Qilian Shan, and 6.3 (3.5) km/s in the West-Qinling Shan and Songpan-Ganzi terrane. Beneath the Tibetan plateau, the average crustal P-wave velocity amounts to 6.38 km/s which is slightly lower than the global average of 6.45 km/s (Christensen and Mooney, 1995).

Velocities in the near-surface layer, i.e. between the surface and interface B, are $V_p=(3.5–5.4)$ km/s ($V_s=2.0–2.7$ km/s) whereby the lowest values are observed in the sedimentary cover of the Ordos basin. The 0–5 km deep, near-surface layer is thick beneath basins and thin or completely missing beneath uplifted areas.

The upper crystalline crust is divided into an upper and lower normal gradient layer by interface C_1. Velocities vary between $V_p=5.7–6.1$ km/s ($V_s=3.15–3.55$ km/s) in the upper layer (between interface B and C1 in Fig. 6a and b) and between $V_p=6.0–6.3$ km/s ($V_s=3.6–3.7$ km/s) in the lower layer (between interface C1 and C in Fig. 6a and b). We observe low velocity zones (LVZ) with $V_p<6.2$ km/s ($V_s<3.5$ km/s) beneath the Haiyuan arcuate tectonic region and the Qinling-Qilian fold system, where the Conrad discontinuity (interface C in Fig. 6a and b) is a laminated interface, and not a sharp boundary.

The lower crust ranges from the Conrad discontinuity (interface C in Fig. 6a and b) to the crust-mantle boundary (interface M in Fig. 6a and b) and includes the interfaces C_3, C_4, and C_5. The NE–SW-increase in lower-crustal thickness is accompanied by further sublayering (interfaces C_3, C_4, and C_5 in Fig. 6a and b). Beneath the Ordos basin velocities increase with depth from $V_p=6.4$ km/s ($V_s=3.7$ km/s) at the top of the lower crust to $V_p=6.8$ km/s ($V_s=3.9$ km/s) at the base of the lower crust. Beneath the Haiyuan arcuate tectonic region interface C_4 divides the lower crust into an upper part with $V_p=6.45–6.5$ km/s ($V_s=3.55$ km/s) and a lower part with $V_p=6.6–6.8$ km/s ($V_s=3.65$ km/s). Here, S-wave velocities are much lower than in the adjacent areas, and the crust–mantle boundary is a laminated interface and shows a step-like interruption beneath SP7. Further to the southwest, beneath the Qinling-Qilian fold system, the lower crust is further subdivided and shows three layers with, from top to bottom, $V_p=6.45$ km/s ($V_s=3.7$ km/s), $V_p=6.5$ km/s ($V_s=3.7–3.8$ km/s), and $V_p=6.7–6.8$ km/s ($V_s=3.8–3.9$ km/s). Southwest of SP2, beneath the Songpan-Ganzi terrane and the West-Qinling Shan, the lower crust shows a subdivision into four layers. The velocity structure is characterized by horizontal low-velocity zones in each of the four layers. The crust–mantle boundary is a laminated interface and shows a step-like interruption beneath SP2.

The velocity in the upper-most mantle is $V_p=7.9–8.0$ km/s ($V_s=4.4–4.6$ km/s). This range is in excellent agreement with previous seismological studies (e.g., Liang et al., 2004; Sun et al., 2004a,b; Hearn et al., 2004).

4.2. Poisson's ratio

Poisson's ratio, σ (or equivalently, V_p/V_s), has been used to determine the crustal composition within the continental crust (e.g., Holbrook et al., 1992; Christensen and Mooney, 1995; Rudnick and Fountain, 1995; Zandt and Ammon, 1995; Christensen, 1996; Catchings and Lee, 1996; Musacchio et al., 1997; Kern et al., 1999; Swenson et al., 2000; Wang et al., 2003). Based on the P-wave and S-wave velocity structure along the Darlag–Lanzhou–Jingbian profile (Fig. 6a and b) the distribution of Poisson's ratio within the crust and upper mantle was obtained (Fig. 6c).

Along the profile, Poisson's ratio varies with depth and distance. The Poisson's ratio ranges between 0.26–0.36 in the near-surface sedimentary cover (between the surface and interface B in Fig. 6c) whereby the high values result from saturated or loosened sediments, or from fractured bedrocks. Poisson's ratio is generally 0.24–0.26 in the upper crust (between interface B and C in Fig. 6c) and 0.25–0.27 in the lower crust (between interface C and M in Fig. 6c), excluding the zones of

Fig. 6. Two-dimensional crustal velocity structure along the Darlag–Lanzhou–Jingbian profile reaching from the Songpan-Ganzi terrane in the southwest to the Ordos basin in the northeast. The top panel shows the tectonic units, faults, and thrust which are crossed by the profile. (a) Crustal P-wave velocity model (V_p), (b) crustal S-wave velocity model (V_s), and (c) Poisson's ratio σ (equivalently, V_p/V_s ratio). The top of the crystalline basement is indicated by "B," the Conrad discontinuity by "C", and the crust–mantle boundary by "M." The upper crust lies between interface "B" and "C", and the lower crust between interface "C" and "M". "C1" and "C3" to "C5" indicate further interfaces in the upper and lower crust, respectively. The cross-sections are shown with a vertical exaggeration of 1:5.

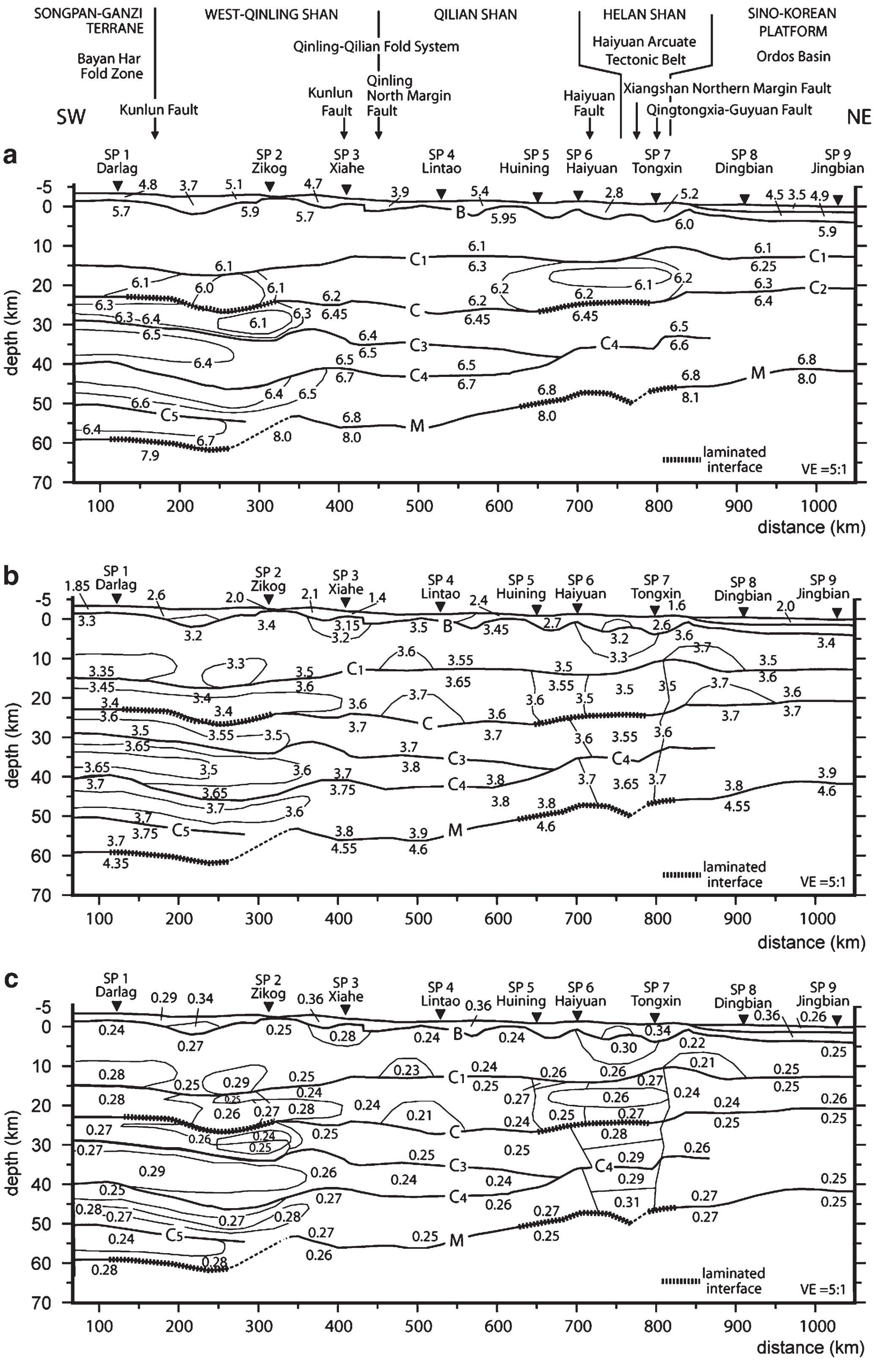
SONGPAN-GANZI TERRANE
WEST-QINLING SHAN
QILIAN SHAN
HELAN SHAN
SINO-KOREAN PLATFORM
Bayan Har Fold Zone
Qinling-Qilian Fold System
Haiyuan Arcuate Tectonic Belt
Ordos Basin
Kunlun Fault
Kunlun Fault
Qinling North Margin Fault
Haiyuan Fault
Xiangshan Northern Margin Fault
Qingtongxia-Guyuan Fault
SW
NE
a
b
c
SP 1 Darlag
SP 2 Zikog
SP 3 Xiahe
SP 4 Lintao
SP 5 Huining
SP 6 Haiyuan
SP 7 Tongxin
SP 8 Dingbian
SP 9 Jingbian
B
C1
C2
C
C3
C4
C5
M
depth (km)
distance (km)
laminated interface
VE =5:1

locally high or low Poisson's ratio. Within the upper crust we observe, locally, zones of low σ-values ($\sigma<0.23$) beneath the Qilian Shan which can be linked to zones of high S-wave velocities ($V_s>3.6$ km/s). Zones of locally high σ-values with $0.27<\sigma<0.29$ in the upper crust and $0.27<\sigma<0.31$ in the lower crust are apparent beneath the Songpan-Ganzi terrane, the West-Qinling Shan and the Haiyuan arcuate tectonic region. Beneath the Songpan-Ganzi terrane and the West-Qinling Shan zones of high σ-value ($\sigma>0.28$) alternate with zones of average σ-value. The high-σ anomalies correlate with zones of low P- and S-wave velocities with the exception of the top layer of the upper crust (between interface B and C1 in Fig. 6) where high σ-values are caused by low S-wave velocities. The crust beneath the Haiyuan fault, the Xiangshan Northern Margin fault, and the Qingtongxia–Guyuan faults is transected by a ~100-km-wide zone of high σ-values which extends to the base of the crust. In the upper and lower crust ó-values are 0.26–0.30 and 0.28–0.30, respectively. Here, high σ-values correlate with low S-wave velocities except for the lower layer of the upper crust where we also observe low P-wave velocities.

5. Discussion

The Tibetan plateau has the thickest crust and the highest elevation on the Earth, and many large earthquakes occur in the region surrounding the plateau. One of the largest in recent times was the 1920 $M=8.5$ Haiyuan earthquake at the NE margin of the plateau. Inferences about the crustal composition and mechanisms of thickening and uplift of the plateau raise controversial questions. Using the results of the seismic refraction survey along the Darlag–Lanzhou–Jingbian profile, we discuss these questions below.

5.1. Crustal composition

There are two approaches to determine the crustal composition from seismic velocities. The first approach uses P-wave velocity intervals to identify sedimentary and basement rocks ($V_p<5.7$), as well as felsic ($5.7<V_p\leq 6.4$), intermediate ($6.4<V_p\leq 6.9$) and mafic ($6.9<V_p\leq 7.3$) material within the crust (Christensen and Mooney, 1995). The second approach is based on the relationship between V_p–σ-value and crustal composition.

The crustal composition as identified through P-wave velocity intervals is shown in Fig. 7. The crust consists of a felsic upper and an intermediate lower crust except in the Songpan-Ganzi terrane and the West-Qinling Shan. Here, the lower crust is laminated with alternating felsic and intermediate layers. The more felsic composition of the Songpan-Ganzi terrane is also reflected in the low average P-wave velocity of 6.3 km/s.

The composition of the crust derived from V_p–σ-values shows that the different layers of the crust have,

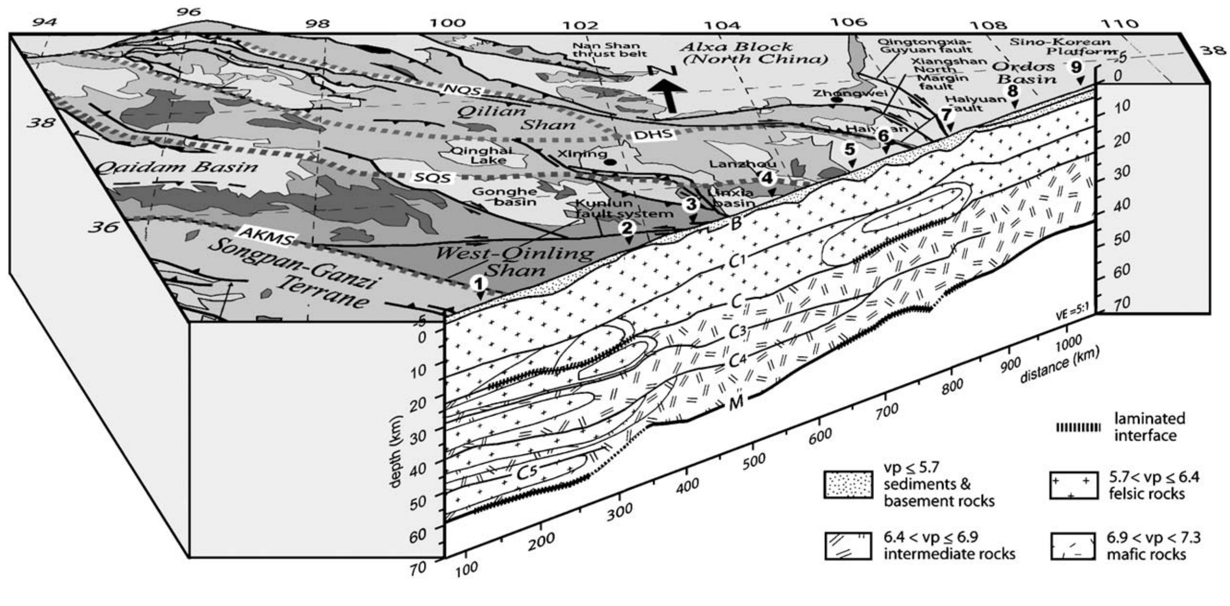

Fig. 7. Three-dimensional perspective view of the compositional structure of the crust along the Darlag–Lanzhou–Jingbian profile. The composition is derived from the P-wave velocity structure (Fig. 6a) whereby felsic, intermediate, and mafic material is identified through velocity intervals according to Christensen and Mooney (1995). For discussion see text.

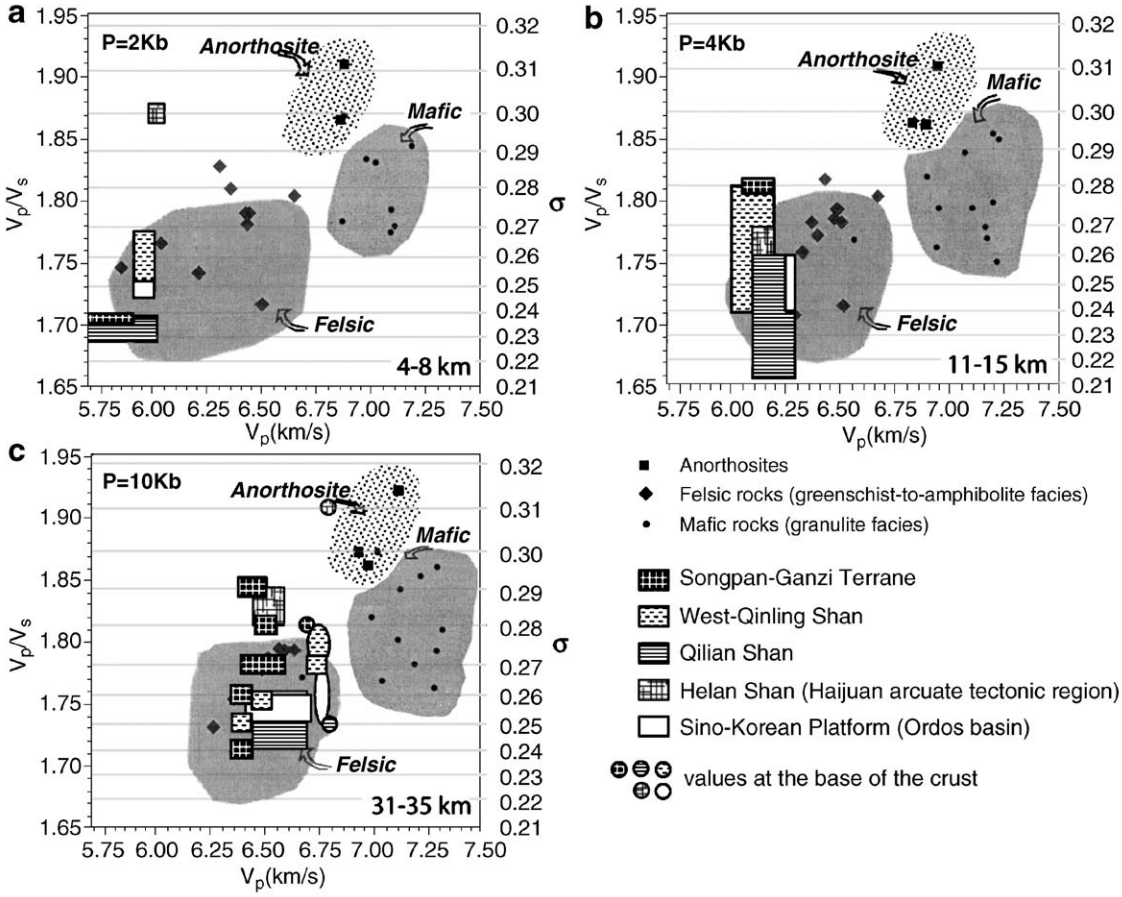

Fig. 8. Poisson's ratio σ (equivalently, V_p/V_s) versus P-wave velocity V_p at pressures characteristic for the (a) 4–8 km depth (2 kb), (b) 10–14 km depth (4 kb) and (c) 31–35 km depth (10 kb). Gray-shaded areas indicate domains of felsic, mafic and anorthositic composition as derived from laboratory measurements on rock samples (solid symbols) (Musacchio et al., 1997). The range of V_p–σ-values for the (1) Songpan-Ganzi terrane, (2) West-Qinling Shan, (3) Qilian Shan, (4) Haiyuan arcuate tectonic region, and (5) Ordos basin are shown in different patterns. In (a) and (b), we plotted the V_p–σ-values for the upper and lower layer of the upper crust, respectively. In (c) we plotted the V_p–σ-ranges for the lower crust and at the base of the crust. For the Songpan-Ganzi terrane and the West-Qinling Shan, several V_p–σ-values indicate that here the lower crust is laminated. For discussion see text.

in general, a felsic composition which changes into a more intermediate composition at the base of the crust (Fig. 8). Notably, V_p–σ-values fall outside the areas of classified composition for the crust beneath the Songpan-Ganzi terrane, the West-Qinling Shan, and the Haiyuan arcuate tectonic region. These areas of anomalous V_p–σ-values can be correlated with major strike-slip faults along the profile, i.e. the Kunlun fault system, the Haiyuan fault, the Xiangshan Northern Margin fault, and the Qingtongxia-Guyuan faults. In the crust beneath the Haiyuan arcuate tectonic region, high σ-values are caused by low S-wave velocities (Fig. 8b) which could indicate the presence of fluids. Along the profile, high heat flow of 60–66 mW/m^2 (Wang, 2001) could produce temperatures in the lower crust that exceed the solidus for felsic material and result in partial melting. Partial meting causes a decrease in S-wave velocity and, consequently, an increase in Poisson's ratio. Thus, high σ-values at lower crustal depth could indicate partial melting. In contrast, the high σ-values beneath the Songpan-Ganzi terrane and the West-Qinling Shan result from the combination of low P- and S- wave velocities (Fig. 8a and b).

Along the profile, large-scale strike-slip faults and laminated Conrad and Moho interfaces correlate with areas of anomalous V_p–σ-values. This suggests that partial melting is likely a result of tectonic activities. Partial melting is thought to exist in other regions of the Tibetan plateau as well. Other seismological studies show that the crust of the northern Songpan-Ganzi terrane and the northern Qiangtang are characterized by low S-wave velocities and a high Poisson's ratio

(McNamara et al., 1994; Owens and Zandt 1997). Seismological observations, together with the presence of hot springs and high electrical conductivity (Wei et al., 2001; Unsworth et al., 2004) have been interpreted to indicate that the lower crust of the central Tibetan plateau is undergoing partial melting (Yin and Harrison, 2000). Galve et al. (2002), however, think that there is no significant partial melting in the deep crust.

The felsic composition of the crust beneath the northeastern Tibetan plateau is consistent with the results of Galve et al. (2002), Vergne et al. (2002) and Wang et al. (in press). Young orogens usually have felsic crustal composition. Zandt and Ammon (1995) find that, on average, Poisson's ratio increases with the age of the crust. Their results strongly support the presence of a mafic lower crust beneath cratons. The Ordos basin is a craton with an Archean basement, where the crustal thickness of 42 km correlates well with the global average of 41.5 km beneath shields and platforms (Christensen and Mooney, 1995). In the Ordos basin, however, the inferred crustal composition is more felsic than the global average and a mafic lower crust may possibly be absent since the P-wave velocity (6.4–6.8 km/s) and Poisson's ratio (0.25) are both low in the lower crust. In fact, other results from China are contradictory to generally accepted global crustal models of a mafic lower crust (Gao et al., 1998). In recent review articles concerning the seismic properties and composition of the lower crust, studies have been biased towards North America, Western Europe and Australia (Holbrook et al., 1992; Christensen and Mooney, 1995; Rudnick and Fountain, 1995). Those from China were seldom considered (Gao et al., 1998). Likewise, delamination of the lower continental crust has also been proposed as a way to account for the felsic-intermediate composition of the continental crust (Rudnick, 1995).

5.2. Crustal thickening

There are two different end-member models for crustal thickening in the Tibetan plateau. The first model assumes that thickening occurs mainly in the lower crust. Clark and Royden (2000) point out that the lack of significant upper crustal shortening across much of the eastern plateau margin implies that crustal thickening occurs mainly in the deep crust by lower crustal flow. Wang et al. (2003) suggest that if the crust has been thickened by magmatic additions that were mainly of intermediate to mafic composition, then thickening would have primarily occurred in the middle and lower crust. The second model assumes that thickening occurs mainly in the upper crust. Galve et al. (2002) argue that north of the Kunlun fault, in the Qinling-Qilian fold system, the thickening of only the upper crust is implied by the dominantly felsic crustal composition. Vergne et al. (2002) hypothesize that the relatively small thickness of this mafic lower crust supports the idea that the thickening and shortening of the northeastern Tibetan crust is preferentially accommodated in the weak, upper felsic regions.

Our results support thickening in both the upper and lower crust. On the one hand, the results of the Darlag-Lanzhou-Jingbian profile show that the thickness of the lower crust increases from 22 to 38 km when the crustal thickness increases from 42 km in the Ordos basin to 63 km in the Songpan-Ganzi terrane south of the Kunlun fault. The results of shot point SP1 show there is a high and low velocity interbedded structure in the lower crust of the Songpan-Ganzi terrane, indicating that the lower crust is the main region of deformation and thickening (Zhang et al., 2003). We suggest that dominantly felsic crustal composition does not necessarily indicate thickening of only the upper crust because most of the mafic layer in the bottom of the thickened lower crust might have been stripped away from the lithosphere by delamination. Therefore, we believe thickening occurs primarily in the lower crust.

5.3. Tectonic activities

Evidence of tectonic activity is readily apparent when the seismic profile crosses the NS Belt and Central Orogenic Belt in China. Part of the Central Orogenic Belt is the West-Qinling Shan, where the thickness of the lower crust sharply increases and there are LVZs and possible partial melting. The NS Belt passes through the Haiyuan arcuate tectonic region, where there are also LVZs, as well as obvious variations of crustal thickness, complicated fault types, and large earthquakes.

In 1920, an $M = 8.5$ earthquake occurred in the Haiyuan arcuate tectonic region, between the active northeastern Tibetan plateau and two tectonic stable regions (the Sino–Korean platform in the northeast and the Gobi Ala Shan platform in the north). The earthquake's focus was located on the Haiyuan fault, where the crust becomes obviously thicker from northeast to southwest and there is a LVZ. As continued under-thrusting of the Indian plate pushed the Tibetan Plateau to the NE, the Sino–Korean platform and Gobi Ala Shan platform acted as rigid blocks to resist the northeastward motion. As a result, the lower crust of the Tibetan plateau grew vertically as it compacted (Zhu and Helmberger, 1998), and four arcuate faults formed in the Haiyuan arcuate tectonic region under the combined effects of the three geological units. The faults are of sinistral strike-slip motion in the region of divergence, and of compressional thrusting in the region of convergence. Thus, the Haiyuan earthquake occurred on the Haiyuan fault with sinistral strike-slip motion, as well as a compressional thrusting component.

6. Conclusions

The seismic refraction profile in the NE margin of the Tibetan plateau, called the Darlag–Lanzhou–Jingbian profile, crosses the northern Songpan-Ganzi terrane, the Qinling-Qilian fold system including the West-Qinling Shan and Qilian Shan, the Haiyuan arcuate tectonic region, and the Ordos basin. The P- and S-wave velocity structure and Poisson's ratios have been determined, and the main characteristics of the profile are summarized as follows.

(1) The crustal thickness increases from northeast to southwest. The average crustal thickness observed is 42 km beneath the Ordos basin, which correlates well with the global average (41.5 km) for shields and platforms (Christensen and Mooney, 1995). It is 47 km in the Haiyuan arcuate region, 47–56 km in the Qilian Shan, 54–62 km in the West-Qinling Shan and 63 km in the Songpan-Ganzi terrane. The crust becomes abruptly thicker south of the Haiyuan fault and beneath the West-Qinling Shan.

(2) Along the profile the average P-wave velocities of the crystalline crust, i.e. between interface B and M in Fig. 6a, vary between 6.3–6.4 km/s and are 0.05–0.15 km/s lower than the worldwide average of 6.45 km/s [Christensen and Mooney, 1995]. South of the Kunlun fault, beneath the Songpan-Ganzi terrane and the West-Qinling Shan, the average P-wave velocity is low (6.3 km/s). North of the Kunlun fault, beneath the Ordos basin and the Qilian Shan, the average P-wave velocity is 6.4 km/s. Beneath the Haiyuan arcuate tectonic region the average P-wave velocity shows a local minima of 6.3 km/s.

(3) The crust has felsic composition. Combined P-wave velocities and Poisson's ratios suggest that there is dominantly felsic composition in the crust and an intermediate composition at the base of the crust, with a mafic lower crust likely absent in the NE margin of the Tibetan plateau, from the Songpan-Ganzi terrane to the Ordos basin.

(4) There are low velocity zones in the West-Qinling Shan and in the Haiyuan arcuate tectonic region. The low velocity zones have low S-wave velocities and high Poisson's ratios, so it is possible that these low velocities result from partial melting.

(5) The crust is divided into two layers, the upper and the lower crust, with crustal thickening occurring mainly in the lower crust in the NE Tibetan plateau. The results in the study show that the thickness of the lower crust increases from 22 to 38 km when the crustal thickness increases from 42 km beneath the Ordos basin to 63 km in the Songpan-Ganzi terrane south of the Kunlun fault.

(6) There are anomalous structures in the crust of the West-Qinling Shan and in the Haiyuan arcuate tectonic region. Both the Conrad interface and Moho in the two regions are laminated, indicating intense tectonic activity. The arcuate faults and large earthquakes in the Haiyuan arcuate tectonic region are the result of interactivity between the Tibetan plateau and the Sino–Korean and Gobi Ala Shan platforms.

Acknowledgements

The work is sponsored by National Natural Science Foundation of China (Grant No. 40374032). The first and third authors would like to express their appreciation for the support of the scientific exchange program of the U. S. Geological Survey. We thank Jichang Fan and Baofeng Liu for their advice on data processing during the research. The paper benefited from insightful reviews by J. Mechie, S. T. McDonald, M. Coble, and two anonymous reviewers.

References

Catchings, R.D., Lee, W.H.K., 1996. Shallow velocity structure and Poisson's ratios across earthquake source zone from Memphis, Tennessee, to St. Louis, Missouri. Bull. Seismol. Soc. Am. 86, 1704–1713.

Cerveny, V., Psencik, I. (Eds.), 1984. SEI83-numerical modeling of seismic wavefield in 2-D laterally varying layered structures by the ray method. In Engdahl E.R. (Ed.), Documentation of Earthquake Algorithms. Rep. SE-35, World Data Cent. (A) for Solid Earth Geophys., Boulder, Colo., pp. 36–40.

Cerveny, V., Molotkov, I.A., Psencik, I. (Eds.), 1977. Ray Method in Seismology. Univ. Karlova, Prague, pp. 57–158.

Christensen, N.I., 1996. Poisson's ratio and crustal seismology. J. Geophys. Res. 101, 3139–3156.

Christensen, N.I., Mooney, W.D., 1995. Seismic velocity structure and composition of the continental crust: a global view. J. Geophys. Res. 101, 9761–9788.

Clark, M.K., Royden, L.H., 2000. Topographic ooze: building the eastern margin of Tibet by lower crustal flow. Geology 28, 703–706.

Cui, Z., Li, Q., Wu, C., Yin, Z., Liu, H., 1995. The crustal and deep structures in Golmud-Ejin Qi GGT. Acta Geophys. Sin. 38 (Suppl. II), 15–28.

Galve, A., Hirn, A., Jiang, M., Gallart, J., de Voogd, B., Lepine, J.C., Diaz, J., Wang, Y., Qian, H., 2002. Modes of raising northeastern Tibet probed by explosion seismology. Earth Planet. Sci. Lett. 203, 35–43.

Gao, S., Zhang, B.R., Jin, Z.M., Kern, H., Luo, T.C., Zhao, Z.D., 1998. How mafic is the lower continental crust? Earth Planet. Sci. Lett. 161, 101–117.

Giese, P., Prodehl, C., Stein, A. (Eds.), 1976. Explosion Seismology in Central Europe. Springer-Verlag, New York, pp. 146–161.

Hearn, T.M., Wang, S., Ni, J.F., Xu, Z., Yu, Y., Zhang, X., 2004. Uppermost mantle velocities beneath China and surrounding areas. J. Geophys. Res. 109, doi:10.1029/2003JB002874, 11 pp.

Herquel, G., Wittlinger, G., Guilbert, J., 1995. Anisotropy and crustal thickness of Northern Tibet: new constraints for tectonic modeling. Geophys. Res. Lett. 22, 1925–1928.

Holbrook, W.S., Mooney, W.D., Chrisensen, N.I., 1992. The seismic velocity structure of the deep continental crust. In: Fountain, D.M., Arculus, R., Kay, R.W. (Eds.), The Continental Lower Crust. Elsevier Science, New York, pp. 1–43.

Jiang, C.F., Wang, Z.Q., Li, J.Y., 2000. The Opening-Closing Tectonics of the Central Orogenic Belt in China. Geol. Publ. House, Beijing, China. (in Chinese with English abstract).

Kern, H., Gao, S., Jin, Z., Popp, T., Jin, S., 1999. Petrophysical studies on rocks from the Dabie ultrahigh-pressure (UHP) metamorphic belt, Central China: implications for the composition and delamination of the lower crust. Tectonophysics 301, 191–215.

Li, S.L., Mooney, W.D., 1998. Crustal structure of China from deep seismic sounding profiles. Tectonophysics 288, 105–113.

Li, S.L., Zhang, X.K., Zhang, C.K., Zhao, J.R., Cheng, S.X., 2002. A preliminary study on the crustal velocity structure of Maqin–Lanzhou–Jingbian by means of deep seismic sounding profile. Chin. J. Geophys. 45 (2), 210–217 (in Chinese with English abstract).

Liang, C., Song, X., Huang, J., 2004. Tomographic inversion of Pn travel-times in China. J. Geophys. Res. 109, doi:10.1029/2003JB002789.

Liu, B.F, Li, S.L., Zhang, X.K., Zhang, C.K., Ren, Q.F., Hai, Y., 2003. Study of crustal structure with S-wave data from Maqin–Jingbian profile. Acta Seismol. Sin. 16 (1), 92–98.

McNamara, D.E., Owens, T.J., Silver, P.G., Wu, F.T., 1994. Shear wave anisotropy beneath the Tibetan plateau. J. Geophys. Res. 99, 13655–13665.

Meyer, B., Tapponnier, P., Bourjot, L., Métivier, F., Gaudemer, Y., Peltzer, G., Guo Shunmin, Chen Zitai, 1998. Crustal thickening in Gansu-Qinghai, lithospheric mantle subduction and oblique, strike-slip controlled growth of the Tibetan plateau. Geophys. J. Int. 135, 1–47.

Molnar, P., Tapponnier, P., 1975. Cenozoic tectonics of Asia: effects of a continental collision. Science 189, 419–426.

Musacchio, G., Mooney, W.D., Luetgert, J.H., Christensen, N.I., 1997. Composition of the crust in the Greenville and Appalachian provinces of North America inferred from V_p/V_s. J. Geophys. Res. 102, 15,225–15,241.

Owens, T.J., Zandt, G., 1997. Implications of crustal property variations for models of Tibetan plateau evolution. Nature 387, 37–43.

Pares, J.M., Van der Voo, R.R., Downs, W.R., Yan, M., Fang, X., 2003. Northeastward growth and uplift of the Tibetan plateau: magnetostratigrphic insights from the Guide Basin. J. Geophys. Res. 108 (B1), 2017, doi:10.1029/2001JB001349.

Rudnick, R.L., 1995. Making continental crust. Nature 378, 571–578.

Rudnick, R.L., Fountain, D.M., 1995. Nature and composition of the continental crust: a lower crustal perspective. Rev. Geophys. 33 (3), 267–309.

Sun, Y.S., Morgan, D., Toksov, M.N., 2004a. 3D P- and S-velocity models for the crust and uppermost mantle of China by Monte-Carlo adaptive moving window inversion. Seismol. Res. Lett. 74, 202–203.

Sun, Y.S., Li, X., Kuleli, S., Morgan, F.D., Toksov, M.N., 2004b. Adaptive moving window method for 3D P-velocity tomography and its application in China. Bull. Seismol. Soc. Am. 94, 740–746.

Swenson, J.L., Beck, S.L., Zandt, G., 2000. Crustal structure of the Altiplano from broadband regional waveform modeling: implications for the composition of thick continental crust. J. Geophys. Res. 105, 607–621.

Tapponnier, P., Xu, Z.Q., Roger, F., Meyer, B., Arnaud, N., Wittlinger, C., Yang, J.S., 2001. Oblique stepwise rise and growth of the Tibet plateau. Science 294, 1671–1677.

Tian, Q.J., Ding, G.Y., 1998. Characteristics of tectonic region of quasi triple junction in the northeastern corner of Qinghai-Tibetan plateau. Earthq. Res. China 14 (4), 27–35 (in Chinese with English abstract).

Unsworth, M., Wei, W., Jones, A.G., Li, S., Bedrosian, P., Booker, J., Jin, S., Deng, M., Tan, H., 2004. Crustal and upper mantle structure of northern Tibet imaged with magnetotelluric data. J. Geophys. Res. 109 (2) (18 pp.).

Vergne, J., Wittlinger, G., Hui, Q., Tapponnier, P., Poupinet, G., Mei, J., Herquel, G., Paul, A., 2002. Seismic evidence for stepwise thickening of the crust across the NE Tibetan plateau. Earth Planet. Sci. Lett. 203, 25–53.

Wang, Y., 2001. Heat flow pattern and lateral variations of lithospheric strength in China mainland: constraints on active deformation. Phys. Earth Planet. Inter. 126, 121–146.

Wang, Y.X., Mooney, W.D., Yuan, X., Coleman, R.G., 2003. The crustal structure from the Altai Mountains to the Altyn Tagh fault, northwest China. J. Geophys. Res. 108 (B6), 2322, doi:10.1029/2001JB000552.

Wang, Y.X., Mooney, W.D., Yuan, X. Okaya, N., in press. Crustal structure of the northeastern Tibetan plateau from the southern Tarim basin to the Sichuan basin. J. Geophys. Res.

Wei, W., Unsworth, M., Jones, A., Booker, J., Tan, H., Nelson, D., Chen, L., Li, S., Solon, K., Bedrosian, P., Jin, S., Deng, M., Ledo, J., Kay, D., Roberts, B., 2001. Detection of widespread fluids in the Tibetan crust by magnetotelluric studies. Science 292 (5517), 716–718.

Yin, C.Y., 2002. The thickness of seismogenic layer under the areas surrounding the Ordos block, Northern China. Pure Appl. Geophys. 159, 1613–2628.

Yin, A., Harrison, T.M., 2000. Geologic evolution of the Himalayan–Tibetan orogen. Annu. Rev. Earth Planet. Sci. 28, 211–280.

Zandt, G., Ammon, C.J., 1995. Continental crust composition constrained by measurements of crustal Poisson's ratio. Nature 374, 152–154.

Zhang, X.K., Li, S.L., Wang, F.Y., Jia, S.X., Fang, S.M., 2003. Differences of crustal structures in the northeastern edge of Tibet plateau, Ordos and Tangshan earthquake region in north China — results of deep seismic sounding. Seismol. Geol. 25 (1), 53–60 (in Chinese with English abstract).

Zhu, L., Helmberger, D.V., 1998. Moho offset across the northern margin of Tibetan plateau. Science 281, 1170–1172.